The Astrophysical Journal Letters, 934:L5 (6pp), 2022 July 20 https://doi.org/10.3847/2041-8213/ac7ff0


# Radio Constraints on *r*-process Nucleosynthesis by Collapsars

K. H. Lee[1], I. Bartos[1], A. Eddins[2], A. Corsi[2], Z. Márka[3], G. C. Privon[4,5], and S. Márka[6]
[1] Department of Physics, University of Florida, PO Box 118440, Gainesville, FL 32611-8440, USA; imrebartos@ufl.edu
[2] Department of Physics and Astronomy, Texas Tech University, Box 1051, Lubbock, TX 79409-1051, USA
[3] Department of Physics, Columbia University in the City of New York, New York, NY 10027, USA
[4] National Radio Astronomy Observatory, 520 Edgemont Road, Charlottesville, VA 22903, USA
[5] Department of Astronomy, University of Florida, 211 Bryant Space Science Center, Gainesville, FL 32611, USA
[6] Columbia Astrophysics Laboratory, Columbia University in the City of New York, New York, NY 10027, USA
*Received 2022 February 22; revised 2022 June 23; accepted 2022 July 9; published 2022 July 20*

## Abstract

The heaviest elements in the universe are synthesized through rapid neutron capture (*r*-process) in extremely neutron-rich outflows. Neutron star mergers were established as an important *r*-process source through the multimessenger observation of GW170817. Collapsars were also proposed as a potentially major source of heavy elements; however, this is difficult to probe through optical observations due to contamination by other emission mechanisms. Here we present observational constraints on *r*-process nucleosynthesis by collapsars based on radio follow-up observations of nearby long gamma-ray bursts (GRBs). We make the hypothesis that late-time radio emission arises from the collapsar wind ejecta responsible for forging *r*-process elements, and consider the constraints that can be set on this scenario using radio observations of a sample of Swift/Burst Alert Telescope GRBs located within 2 Gpc. No radio counterpart was identified in excess of the radio afterglow of the GRBs in our sample. This gives the strictest limit to the collapsar *r*-process contribution of $\lesssim 0.2\ M_\odot$ for GRB 060505 and GRB 05826, under the models we considered. Our results additionally constrain energy injection by a long-lived neutron star remnant in some of the considered GRBs. While our results are in tension with collapsars being the majority of *r*-process production sites, the ejecta mass and velocity profile of collapsar winds, and the emission parameters, are not yet well modeled. As such, our results are currently subject to large uncertainties, but further theoretical work could greatly improve them.

*Unified Astronomy Thesaurus concepts:* R-process (1324); Gamma-ray bursts (629)

## 1. Introduction

The remarkable multimessenger discovery of the neutron star merger GW170817 by the LIGO (Aasi et al. 2015) and Virgo (Acernese et al. 2015) gravitational-wave observatories and their partners has marked the beginning of a new era in astrophysics (Abbott et al. 2017). Among others, it confirmed that neutron star mergers eject mildly relativistic, neutron-rich matter. This ejecta can produce the heaviest elements known in nature through rapid neutron capture (*r*-process) nucleosynthesis (Chornock et al. 2017; Perego et al. 2017; Pian et al. 2017; Drout et al. 2017).

Based on the ejecta mass from GW170817, neutron star mergers could be the main source of heavy *r*-process elements in the universe. Nevertheless, theoretical and observational uncertainties remain (Bartos & Marka 2019a; Siegel 2019; Kobayashi et al. 2020).

Collapsars—rapidly rotating massive stars whose iron-core collapse produces a black hole (Woosley & MacFadyen 1999)—have also been proposed as a major source of heavy *r*-process elements (Nakamura et al. 2013, 2015; Siegel et al. 2019; Brauer et al. 2021). This possibility could help explain the observed early enrichment of dwarf galaxies (Ji et al. 2016) and the long-term chemical enrichment of the Milky Way (Côté et al. 2017; Hotokezaka et al. 2018). The mass of *r*-process elements produced per event inferred from dwarf galaxy *r*-process data is also consistent with a collapsar origin (Beniamini et al. 2016). Nonetheless, their low rate is in tension with meteoritic *r*-process abundances (Bartos & Marka 2019b), while the observed gradual increase of [Ba/Mg] with [Fe/H] in metal-poor stars also disfavors collapsars (Tarumi et al. 2021).

Fallback accretion onto the newly formed black hole in collapsars could drive winds similar to those observed in neutron star mergers, except with a larger ejecta mass due to more available mass in collapsar accretion disks. This wind outflow, hereafter "collapsar wind ejecta," could become highly neutron-rich due to electron capture reactions on protons (Siegel et al. 2019), enabling it to robustly synthesize even heavy *r*-process elements.

So far, there is no direct evidence of *r*-process nucleosynthesis by collapsars. Such an observation is difficult since most collapsars are much farther than GW170817, and because optical emission from decaying *r*-process elements, which was observed for GW170817, can be outshone by supernovae ignited by the collapsars (Zenati et al. 2020). Hence, it has been difficult to confirm, or rule out, collapsars as major *r*-process production sites.

Collapsar wind ejecta could produce late-time, slowly evolving radio flares driven by the outflow's interaction with the surrounding medium. This radio emission is analogous to the late-time, slowly rising radio flares expected in the case of neutron star mergers (Nakar & Piran 2011; Bartos et al. 2019; Grandorf et al. 2021), which may have already been detected (Lee et al. 2020; Hajela et al. 2022). Collapsars, however, may be more favorable for the detection of radio flares: (i) since they are rarer than neutron star mergers, they individually need to eject more matter than a neutron star merger to explain the

**Table 1**
List of Swift/BAT Long GRBs with Distance <2 Gpc.

| GRB Name | R.A. hh:mm:ss | Decl. dd:mm:ss | Err. ″ | SN | $n$ $cm^{-3}$ | Dist. Mpc | Limit mJy | Freq. GHz | Obs. Date | GCN | $M_{ej}$ | Reference |
|---|---|---|---|---|---|---|---|---|---|---|---|---|
| 191019A | 22:40:5.93 | −17:19:40.9 | 2.4 | ⋯ | ? | 1293 | ⋯ | ⋯ | ⋯ | 26043 | ⋯ | ⋯ |
| 190829A | 02:58:10.57 | −08:57:28.6 | 2.0 | ⋯ | ? | 373 | ⋯ | ⋯ | ⋯ | 25552 | ⋯ | ⋯ |
| 171205A | 11:09:39.37 | −12:35:20.1 | 2.3 | 2017iuk | wind | 168 | 0.5 | 3 | 2020.10.10 | 22179 | 0.5 | 1 |
| 161219B | 06:06:51.36 | −26:47:29.9 | 1.7 | 2016jca | ? | 726 | 0.6 | 3 | 2019.07.04 | 20297 | ⋯ | ⋯ |
| 150727A | 13:35:52.42 | −18:19:32.7 | 1.8 | ⋯ | ? | 1688 | 0.5 | 3 | 2019.06.30 | 18079 | ⋯ | ⋯ |
| 111225A | 00:52:37.34 | +51:34:17.6 | 2.2 | ⋯ | ? | 1589 | 0.02 | 6 | 2017.09.15 | 12724 | ⋯ | ⋯ |
| 061021 | 09:40:35.87 | −21:57:07.2 | 5 | ⋯ | <0.2 | 1898 | 0.5 | 3 | 2019.06.29 | 5746 | ⋯ | 2 |
| 060505 | 22:07:4.5 | −27:49:57.8 | 4.7 | ⋯ | 1* | 422 | 0.5 | 3 | 2020.10.25 | 5081 | 0.15 | 3 |
| 060218 | 03:21:39.7 | +16:52:01.8 | 3.6 | 2006aj | <30 | 150 | 0.5 | 3 | 2019.03.24 | 4786 | ⋯ | 2 |
| 051109B | 23:01:50.35 | +38:40:49.6 | 4 | ⋯ | <0.2 | 377 | 0.4 | 3 | 2019.04.13 | 4226 | ⋯ | 2 |
| 050826 | 05:51:01.3 | −02:38:41.9 | 6 | ⋯ | $10-10^4$ | 1589 | 0.5 | 3 | 2020.08.15 | 3889 | ⋯ | 2 |

**Note.** For GRBs where $n$ was found from the literature, we indicate the $1\sigma$ confidence interval of the reconstructed $n$ value. Where the lower end of this range is $<10^{-4}$ we only indicate an upper limit. *For GRB 060505 we found the best-fit value, which we indicate, but not the uncertainty of this estimate. For GRBs for which an estimate of $n$ was not found in the literature, our afterglow fit dot not significantly limit $n$, which we indicated with a question mark ("?"). For GRB 171205A, the best fit is a wind profile. Dist.: luminosity distance is converted by using the Planck 2018 results (Aghanim et al. 2018). GCN: number for GRB localization. Ref.: where $n$ and distance are taken from: (1) Leung et al. (2021), (2) Ryan et al. (2015), (3) Xu et al. (2009).

observed abundance of *r*-process elements in the universe, and (ii) they are typically found in a denser interstellar medium (ISM) than neutron star mergers, potentially leading to brighter radio flares.

The emergence, or lack, of a late-time, slowly evolving radio flare could provide observational evidence for or against a mildly relativistic collapsar wind ejecta and could help constrain *r*-process nucleosynthesis by collapsars. This picture may nevertheless be complicated by other outflows from collapsing massive stars, including the beamed, relativistic ejecta that produces gamma-ray bursts (GRBs), and the supernova explosion that ejects a part of the stellar envelope. The emergence of GRBs poses a limited challenge to the interpretation of collapsar radio flares, as radio emission from relativistic outflows that produce the GRBs peak much earlier. In addition, the properties of the relativistic ejecta can be inferred from the observation of the GRB and its afterglow; therefore, it can be accounted for in the interpretation of an observed long-term radio signal.

The effect of supernovae on the observability of collapsar radio flares is less clear. Supernovae contain much more kinetic energy than GRB jets, albeit they expand at a much lower velocity ($\lesssim$0.1 c). Low velocity means that the supernova ejecta leads to a radio flare that peaks only decades after supernova onset (Barniol Duran & Giannios 2015; Lopez-Camara et al. 2022). While long-lasting radio emission peaking at late times has been observed in broad-lined Type Ic supernovae (the same type of supernovae associated with GRBs) strongly interacting with the circumstellar medium (e.g., PTF11qcj; Corsi et al. 2016), no radio rebrightening associated with GRB–supernova events has been identified so far (Peters et al. 2019). However, exceptions are possible. Thus, in the case of a detection compatible with a collapsar radio flare, expectations from an associated supernova needs to be examined. It will also be important to seek further broadband radio follow-up to characterize the spectral properties of the radio emission.

Some observed long GRBs are detected without a coincident supernova even with very deep observations (Eftekhari et al. 2021). There are also reports of the disappearance of a red supergiant after a recent outburst, consistent with a failed supernova (Basinger et al. 2020). Therefore, it is possible that some collapsars do not produce supernovae. If a GRB is observed from the collapsar, it is also possible that the line of site from the collapsar is "cleared" from the exploding stellar envelope, and therefore the collapsar wind ejecta also leaves without significant interference.

We investigated the observational constraints on the collapsar wind ejecta that could be connected to the synthesis of *r*-process elements. We considered detected nearby long GRBs and placed limits on their ejecta properties using existing radio follow-up observations.

## 2. Gamma-Ray Burst Sample

To construct a sample of promising targets, we identified long GRBs that were detected by the Burst Alert Telescope (BAT) on board the Neil Gehrels Swift Observatory (Krimm et al. 2013). Swift/BAT provides accurate localization for follow-up observations. We only considered publicly available afterglows and reconstructed distances. We down-selected this sample to GRBs within 2 Gpc, which could be the brightest sources due to their vicinity. We found 13 GRBs that satisfied these conditions. As we were interested in possible follow-up observations with the Karl G. Jansky Very Large Array (VLA), we discarded two GRBs that fell outside the sky region accessible to the VLA (GRBs 180728A and 060614). The remaining 11 GRBs and their properties are listed in Table 1.

## 3. Ejecta and Radio Emission Model

We modeled radio emission due to the interaction of the collapsar wind ejecta and the surrounding medium following the prescription of Piran et al. (2013). The velocity profile of the collapsar wind ejecta is currently uncertain (e.g., Zenati et al. 2020). We considered two possible velocity profiles. As our fiducial model, we adopted the velocity distribution obtained by Fernández et al. (2019), who carried out a three-dimensional, general-relativistic magnetohydrodynamic (GRMHD) simulation of black hole accretion disks. The simulation was continued long enough to achieve the completion of mass ejection from the disk. This study was motivated by neutron star mergers; however, the black hole–accretion disk configuration is similar in the collapsar case. For comparison we also considered a second model in which the velocity profile of the disk wind follows a power-law distribution. For this distribution, we adopted a power-law index of $\alpha = 4.5$ based on the results of Hajela et al. (2022), and limited the velocity to above $v_{\rm min} = 0.35c$, similar to that of Hajela et al. (2022).

We additionally took into account the effect of the GRB ejecta on the outflow, which can alter the observable radio flare (Margalit & Piran 2020). We injected a relativistic outflow component with initial kinetic energy equal to that obtained for the given GRB based on its afterglow. While this outflow is initially highly beamed, due to the large time frames of interest here and for simplicity we assumed that this outflow is isotropic.

In our simulation, ejecta components with different velocities begin their outflow simultaneously. The initially higher-velocity components expand faster; therefore, they will be the first to interact with the circumburst medium. Slower components therefore expand in empty space until they catch up with the ejecta front that gradually slows as it accumulates more mass from the circumburst medium.

Our standard assumption was that the interstellar medium near the collapsar is initially uniform, with baryon number density $n$, unless the afterglow fit indicated a wind-like density profile. For uniform density, when the ejecta expands out to a radius $R$, it will accumulate $4/3\pi R^3 n m_{\rm p} + M_{\rm ej}(\beta)$ mass from the surrounding medium. Here, $M_{\rm ej}(\beta)$ is the part of the ejecta mass with initial velocity $\geqslant \beta$. This can be used to compute $\beta = \beta(R)$ using energy conservation (Piran et al. 2013)

$$M(R)(\beta c)^2 \approx E(\geqslant\beta), \tag{1}$$

where $E(\beta)$ is the total kinetic energy of the part of the ejecta mass with initial velocity $\geqslant \beta$. We computed $\beta(R)$ by solving Equation (1) numerically, which was then used to obtain $R(t) = \int_0^t \beta(R)dt$, where $t$ is time since the start of the outflow. The typical electron synchrotron frequency in the shock produced by the ejecta medium interaction is (Piran et al. 2013)

$$\nu_{\rm m}(t) \approx 1\ {\rm GHz} \cdot n_0^{\frac{1}{2}} \epsilon_{\rm B,\,-1}^{\frac{1}{2}} \epsilon_{\rm e,\,-1}^{2} \beta(t)^5, \tag{2}$$

while the self-absorption frequency is

$$\nu_{\rm a}(t) \approx 1\ {\rm GHz} \cdot R_{17}(t)^{\frac{2}{p+4}} n_0^{\frac{6+p}{2(p+4)}} \epsilon_{\rm B,\,-1}^{\frac{2+p}{2(p+4)}} \epsilon_{\rm e,\,-1}^{\frac{2(p-1)}{p+4}} \beta(t)^{\frac{5p-2}{p+4}}. \tag{3}$$

Here, $p$ is the electron Lorentz factor power-law index. The parameters $\epsilon_{\rm B}$ and $\epsilon_{\rm e}$ are the fractions of the total internal energy of the shocked gas carried by the magnetic fields and electrons.

For GRBs where an afterglow fit was not available, we used the *Afterglowpy* package (Ryan et al. 2020) to generate afterglow lightcurves. We used the trimmed data set of UKSSDC X-ray telescope (XRT) lightcurves, which is available from the Swift/XRT catalog. Each time of the generation of a lightcurve, the flux density obtained from *Afterglowpy* was integrated with spectral function over the XRT frequency range (0.3—10 keV) to obtain the flux. Then, we performed the Markov Chain Monte Carlo (MCMC) analysis by using the parallel tempering method where the ensembles are run through the likelihoods of $p(D/\Theta)^{1/T}$, where $T$ is the temperature and $\Theta = (\theta_v, E_{iso}, \theta_c, n, p, \varepsilon_e, \varepsilon_{\rm B})$. Using *Afterglowpy*, we adopted a top-hat jet-like afterglow structure as in the example. For data fitting, we used the *ptemcee* package (Foreman-Mackey et al. 2013; Vousden et al. 2016) to perform the parallel tempering ensemble MCMC method, and the bound on uniform prior for $\log_{10} n$ and $p$ is set to be $[-5,3]$ and $[2,3]$, respectively. Initial reference for walkers was set to be random values within [0, 0.02]. From this reference point, we sampled 200 walkers for 20 temperatures each. We first generated 1000 iterations of the "burn-in" process, then we sampled the afterglow lightcurves with 1000 iterations.

We found that the uncertainties obtained for the GRBs where a fit was not available in the literature are large, and the constraints are not substantially different from our prior distributions. In addition, we found that the GRBs for which estimated parameters are available from the literature give stricter constraints on the ejecta mass for the same ($p$, $\epsilon_{\rm B}$, $\epsilon_{\rm e}$). Therefore, in the following we do not consider these GRBs in our ejecta constraints.

For simplicity, we assumed that, for a given event, the values $\epsilon_{\rm B}$ and $\epsilon_{\rm e}$ for the collapsar wind radio flare are the same as for the GRB forward shock. These values are uncertain, but generally do not need to be the same for the two cases. We also explored the results dependence on these values (see Section 5).

For the relevant observing frequency $\nu_{\rm obs}$ and time in our analysis, we have $\nu_{\rm obs} > \nu_{\rm a} > \nu_{\rm m}$, for which the expected flux can be written as

$$F_{\rm obs}(t) = 500\ \mu{\rm Jy}\ R(t)_{17}^3 n_{-1}^{3/2} \beta(t)^1 d_{27}^{-2} \left(\frac{\nu_{\rm obs}}{\nu_m(t)}\right)^{-\frac{p-1}{2}}. \tag{4}$$

## 4. Radio Constraints from Observations

We examined observations in three radio surveys: the Faint Images of the Radio Sky at Twenty Centimeters (FIRST) survey conducted from 2009 to 2011 over the southern Galactic hemisphere with a typical rms sensitivity of 0.15 mJy (Becker et al. 1995), and two observing epochs of the Karl G. Jansky Very Large Array Sky Survey (VLASS) with typical rms sensitivity of 120 $\mu$Jy (Lacy et al. 2020). We utilized the *Photutils* package (Bradley et al. 2020) to estimate the background noise of each GRBs' VLASS Quick-view image above $3\sigma$ after masking possible radio sources.

In addition to the above surveys, GRB 111225A was also observed with a dedicated VLA follow-up in 2017 (Eftekhari et al. 2021).

Only one of the considered GRBs had a reported radio counterpart: GRB 171205A (Leung et al. 2021). The radio afterglow candidate was detectable at least until 900 days post-burst. Comparing to early afterglow detections they found that all radio observations can be explained by afterglow emission

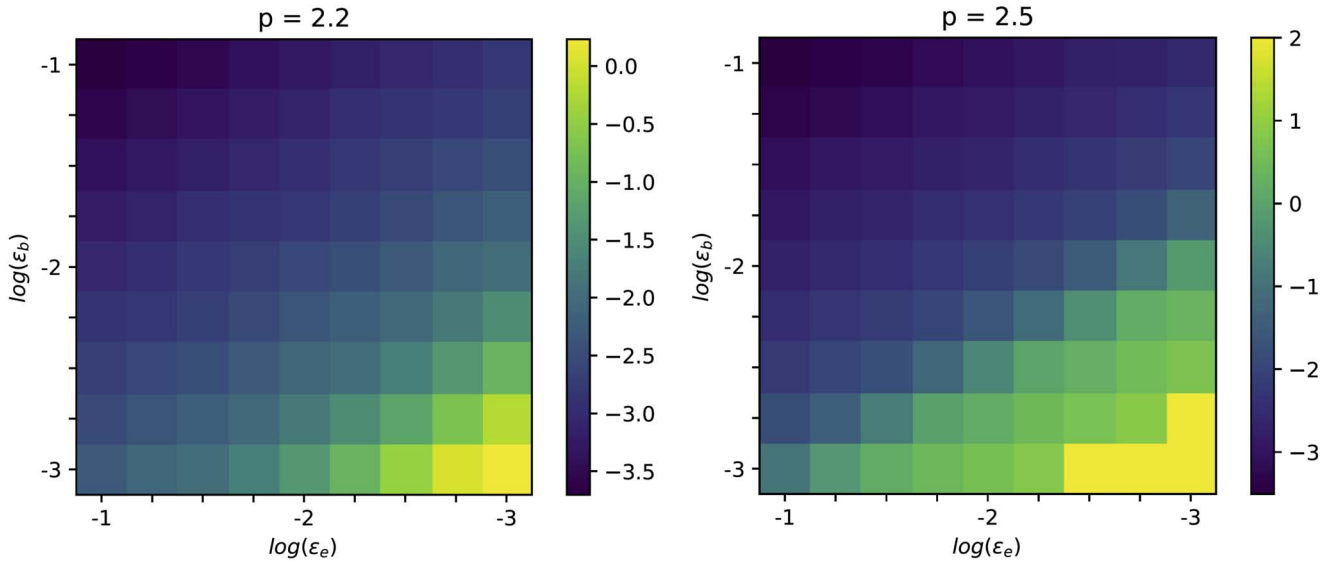


**Figure 1.** Lower limit of circumburst medium density $n$ for which 0.1 $M_\odot$ ejecta mass can be ruled out as a function of $\epsilon_e$ and $\epsilon_B$. We show results for the "GRMHD" ejecta profile; we obtain similar results for the "Power law" ejecta profile. We show results for the electron Lorentz factor power-law index $p = 2.2$ (left) and $p = 2.5$ (right).

propagating in a wind medium and with an unusually high electron Lorentz factor power-law index $p \approx 2.8$.

For each GRB in our sample, the time and observed radio flux limit of the most constraining observation is presented in Table 1. In the case of GRB 171205A, the Table presents the latest nondetection obtained after the reported detection in Leung et al. (2021).

## 5. Constraints on the Ejecta Mass

We used the obtained radio constraints to limit the collapsar wind ejecta mass from each GRB. We computed the expected radio flux at the time of the observation for the GRBs for ejecta masses within $10^{-3} - 2\ M_\odot$. We additionally investigated how the expected radio flux depends on afterglow parameters $\{n, \epsilon_e, \epsilon_B\}$, given their uncertain determination from the afterglow.

We found that one, GRB 060505, is inconsistent with ejecta mass $>0.15\ M_\odot$ ($> 0.05\ M_\odot$) for our fiducial model with $p = 2.5$ ($p = 2.2$). These limits used the best-fit values $\{n = 1\ \mathrm{cm}^{-3}, \epsilon_e = 0.1, \epsilon_B = 0.006\}$ based on the afterglow. To understand how the mass constraint for GRB 060505 depends on the afterglow parameters, we computed the minimum $n$ density for which the ejecta mass can be constrained below 0.1 $M_\odot$ as a function of $\epsilon_e$ and $\epsilon_B$. Our results are shown in Figure 1. We see that our constraint holds for GRB 060505 even if $n$ changes by an order of magnitude for the same $\epsilon_e$ and $\epsilon_B$, or alternatively, the same constraint holds for $n = 1\ \mathrm{cm}^{-3}$ as long as $\epsilon_e \epsilon_B \gtrsim 10^{-4}$. To demonstrate this constraint and the expected uncertainties due to our model, we show possible radio lightcurves at 6 GHz in Figure 2. We see that the velocity profile and different choices for $p$ can significantly alter the lightcurve.

GRB 050826 is another interesting case for which the afterglow fit shows a very high circumburst density of $10 - 10^4\ \mathrm{cm}^{-3}$. Accounting for this uncertain $n$, we found that observations rule out an ejecta mass of 0.1 $M_\odot$ if $\epsilon_e \epsilon_B \gtrsim 10^{-4}$ and $p = 2.2$ or if $\epsilon_e \epsilon_B \gtrsim 10^{-3}$ and $p = 2.5$.

For fixed emission parameters and $n$, our strictest constraints would come from GRB 060218. Observations of this GRB,

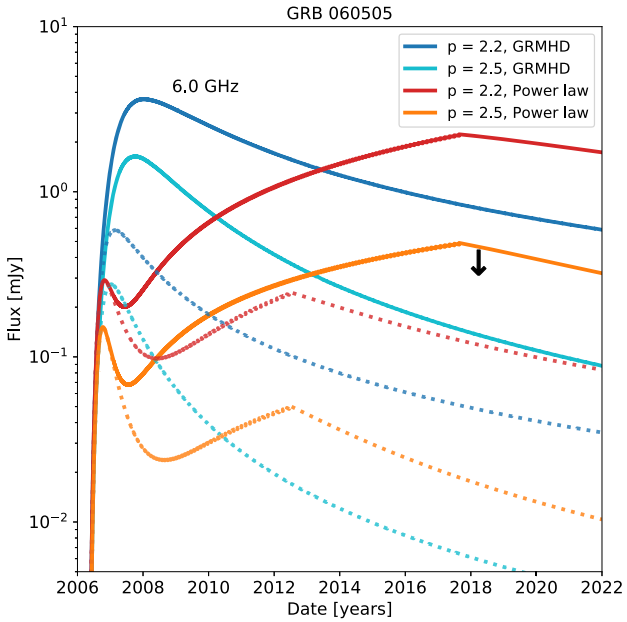


**Figure 2.** Simulated radio lightcurve from the collapsar wind ejecta of GRB 060505 with example parameters. We considered two possible ejecta velocity profiles, "GRMHD" and "Power law" (see the legend and text), two possible values for the electron Lorentz factor power-law index $p$ (see the legend), and two possible ejecta masses: $10^{-1}\ M_\odot$ (solid) and $10^{-2}\ M_\odot$ (dotted). Lightcurves are at 6 GHz. Also shown is an observational constraint obtained by VLA in 2018 (black arrow). The early first peak in the "Power law" case is due to the GRB afterglow, while in the "GRMHD" case the collapsar wind ejecta is much brighter, making the afterglow's effect negligible.

however, poorly constrain $n$, and therefore we do not consider it further here.

For GRB 171205A, instead of our fiducial model of constant circumburst density, we considered a wind model with density decreasing with $r^{-2}$. For this case we adopted the density obtained by Leung et al. (2021) through their fit of the afterglow emission of GRB 171205A. With this model, assuming a terminal shock radius of 1 pc (0.01 pc) beyond which the medium density is taken to be $1\ \mathrm{cm}^{-3}$, we could constrain the ejecta mass to $\lesssim 0.5\ M_\odot$ ($\lesssim 0.05\ M_\odot$).

The flux detected for GRB 171205A (Leung et al. 2021) prior to the latest nondetection reported here does not meaningfully constrain the possible collapsar ejecta mass. If we assume that the latest detection at ∼900 days after the GRB is fully from the collapsar ejecta, i.e., not from the afterglow, we find that the ejecta mass needs to be $>1\,M_\odot$, i.e., a mass less than this cannot be ruled out by the observation.

Long GRBs occur about 4 times less frequently as short GRBs. This means that collapsars need to have a wind ejecta mass of more than about 0.1–0.2 $M_\odot$ to be the major *r*-process sources in the universe, if we adopt the ejecta inferred from GW170817 as typical for neutron star mergers. Even higher ejecta masses (up to $\sim 2\,M_\odot$) are possible under the assumption that black hole accretion in collapsars and neutron star mergers is directly proportional to the radiated $\gamma$-ray energy (Siegel et al. 2019). Our fiducial model with constant-density circummerger medium constraining the ejecta mass is at this threshold. We conclude that with future observations, and the reduction of model uncertainties, radio observations may be a powerful direct means to establish the *r*-process yield of collapsars.

## 6. Discussion

Beyond collapsar wind ejecta that we mainly focused on in this work, the long-term radio emission of collapsars can be enhanced if a long-lived neutron star survives the core collapse and injects some of its rotational energy into the outflow. This injection can be $\sim 10^{52}$ erg of quasi-isotropic energy that accelerates the outflow and increases its radio luminosity (Metzger & Bower 2014). We investigated this scenario by adding $3 \times 10^{52}$ erg of kinetic energy to our simulated collapsar wind ejecta, distributed uniformly among the ejecta mass. We found that, for our fiducial "GRMHD" model, such an energy injection can be ruled out independently of the ejecta mass or the choice of $p$ based on GRB 060505, although for our "Power law" velocity distribution this injection can only be ruled out for $p = 2.2$. GRB 171205A rules out this energy injection for ejected mass $M_{\rm ej} \gtrsim 0.1$, for either of our velocity distribution and choice of $p$. Finally, we rule out energy injection for GRB 050806 for our "GRMHD" model and $p = 2.2$.

The detection of GRBs from collapsars is central to our analysis due to its time/direction trigger and information on the afterglow and circumburst medium. A viable alternative search strategy is to carry out a blind survey in which we look for bright radio flares without any GRBs (Beniamini & Lu 2021). While this limits the information available for each event, the expected number of detections could be significantly higher as beaming is not required in this case. The main challenge with this strategy is the differentiation of radio flares from supernova remnants, neutron star mergers, and collapsars, which is likely only doable if the flare is caught while still rising (Beniamini & Lu 2021).

## 7. Conclusions

We searched for the radio signature of collapsar wind ejecta for 11 nearby (<2 Gpc) well-localized GRBs (<5″). We analyzed radio limits from the FIRST and VLASS surveys and a 2017 follow-up observation of GRB 111225A. We found no coincident radio signals beyond the afterglow of the GRBs, which we used to constrain the mass of collapsar wind ejecta.

Assuming a constant-density interstellar medium around the collapsars, we found that ejecta with $\gtrsim 0.2\ M_\odot$ mass are inconsistent with observations of GRB 060505 for our fiducial model. Similar constraints are obtained for GRB 050826 if we assume $\epsilon_e \epsilon_B \gtrsim 10^{-3}$. Considering GRB 171205A and a wind profile for the circumburst density, we obtain a mass constraint of $\lesssim 0.5\ M_\odot$ ($\lesssim 0.05\ M_\odot$) for a 1 pc (0.01 pc) assumed shock termination radius.

Uncertainties in our result include limited information on the circumburst medium density, uncertainty in some of our model parameters ($p$, $\epsilon_e$, $\epsilon_B$), and possible interference by the stellar matter ejected by the supernova. Further, the ejecta mass and velocity profile of collapsar winds are not yet well modeled. Nonetheless, our results show that long-term radio emission can be a viable option to probe *r*-process nucleosynthesis by collapsars that is difficult through other means.

The authors thank Brian Metzger for useful feedback. The National Radio Astronomy Observatory is a facility of the National Science Foundation operated under cooperative agreement by Associated Universities, Inc. A.C. and A.E. acknowledge support from NSF CAREER award #1455090 and NSF award #1841358. Z.M. and S.M. thank Columbia University in the City of New York. Z.M., S.M., and the Columbia Experimental Gravity group are grateful for the generous support of the National Science Foundation under grant PHY-1708028. I.B. acknowledges the support of the National Science Foundation under grants PHY-1911796 and PHY-2110060, and the Alfred P. Sloan Foundation.

## ORCID iDs

I. Bartos https://orcid.org/0000-0001-5607-3637
A. Corsi https://orcid.org/0000-0001-8104-3536
G. C. Privon https://orcid.org/0000-0003-3474-1125

## References

Aasi, J., Abbott, B.P., Abbott, R., et al. 2015, CQGra, 32, 074001
Abbott, B. P., Abbott, R., Abbott, T. D., et al. 2017, PhRvL, 119, 161101
Acernese, F., Agathos, M., Agatsuma, K., et al. 2015, CQGra, 32, 024001
Aghanim, N., Akrami, Y., Ashdown, M., et al. 2018, A&A, 641, A6
Barniol Duran, R., & Giannios, D. 2015, MNRAS, 454, 1711
Bartos, I., Lee, K. H., Corsi, A., Márka, Z., & Márka, S. 2019, MNRAS, 485, 4150
Bartos, I., & Marka, S. 2019a, Natur, 569, 85
Bartos, I., & Marka, S. 2019b, ApJL, 881, L4
Basinger, C. M., Kochanek, C. S., Adams, S. M., Dai, X., & Stanek, K. Z. 2021, MNRAS, 508, 1156
Becker, R. H., White, R. L., & Helfand, D. J. 1995, ApJ, 450, 559
Beniamini, P., Hotokezaka, K., & Piran, T. 2016, ApJ, 832, 149
Beniamini, P., & Lu, W. 2021, ApJ, 920, 109
Bradley, L., Sipőcz, B., Robitaille, T., et al. 2020, astropy/photutils: 1.0.0, v1.0.0 Zenodo, doi:10.5281/zenodo.4044744, https://zenodo.org/record/4044744
Brauer, K., Ji, A. P., Drout, M. R., & Frebel, A. 2021, ApJ, 915, 81
Chornock, R., Berger, E., Kasen, D., et al. 2017, ApJL, 848, L19
Corsi, A., Gal-Yam, A., Kulkarni, S. R., et al. 2016, ApJ, 830, 42
Côté, B., Belczynski, K., Fryer, C. L., et al. 2017, ApJ, 836, 230
Drout, M. R., Piro, A.L., Shappee, B.J., et al. 2017, Sci, 358, 1570
Eftekhari, T., Margalit, B., Omand, C.M.B., et al. 2021, ApJ, 912, 21
Eftekhari, T., Margalit, B., Omand, C., et al. 2021, ApJ, 912, 21
Fernández, R., Tchekhovskoy, A., Quataert, E., Foucart, F., & Kasen, D. 2019, MNRAS, 482, 3373
Foreman-Mackey, D., Hogg, D. W., Lang, D., & Goodman, J. 2013, PASP, 125, 306
Grandorf, C., McCarty, J., Rajkumar, P., et al. 2021, ApJ, 908, 63
Hajela, A., Margutti, R., Bright, J. S., et al. 2022, ApJL, 927, L17
Hotokezaka, K., Beniamini, P., & Piran, T. 2018, IJMPD, 27, 1842005

Ji, A. P., Frebel, A., Chiti, A., & Simon, J. D. 2016, Natur, 531, 610
Kobayashi, C., Karakas, A. I., & Lugaro, M. 2020, ApJ, 900, 179
Krimm, H. A., Holland, S. T., Corbet, R. H. D., et al. 2013, ApJS, 209, 14
Lacy, M., Baum, S. A., Chandler, C. J., et al. 2020, PASP, 132, 035001
Lee, K. H., Bartos, I., Privon, G. C., Rose, J. C., & Torrey, P. 2020, ApJL, 902, L23
Leung, J. K., Murphy, T., Ghirlanda, G., et al. 2021, MNRAS, 503, 1847
Lopez-Camara, D., De Colle, F., Moreno Mendez, E., Shiber, S., & Iaconi, R. 2022, MNRAS, 513, 3634
Margalit, B., & Piran, T. 2020, MNRAS, 495, 4981
Metzger, B. D., & Bower, G. C. 2014, MNRAS, 437, 1821
Nakamura, K., Kajino, T., Mathews, G. J., Sato, S., & Harikae, S. 2013, IJMPE, 22, 1330022
Nakamura, K., Kajino, T., Mathews, G. J., Sato, S., & Harikae, S. 2015, A&A, 582, A34
Nakar, E., & Piran, T. 2011, Natur, 478, 82
Perego, A., Radice, D., & Bernuzzi, S. 2017, ApJL, 850, L37
Peters, C., van der Horst, A. J., Chomiuk, L., et al. 2019, ApJ, 872, 28
Pian, E., D'Avanzo, P, Benetti, S., et al. 2017, Natur, 551, 67
Piran, T., Nakar, E., & Rosswog, S. 2013, MNRAS, 430, 2121
Ryan, G., Van Eerten, H., MacFadyen, A., & Zhang, B.-B. 2015, ApJ, 799, 3
Ryan, G., Van Eerten, H., Piro, L., & Troja, E. 2020, ApJ, 896, 166
Siegel, D. M. 2019, EPJA, 55, 203
Siegel, D. M., Barnes, J., & Metzger, B. D. 2019, Natur, 569, 241
Tarumi, Y., Hotokezaka, K., & Beniamini, P. 2021, ApJL, 913, L30
Vousden, W., Farr, W. M., & Mandel, I. 2016, MNRAS, 455, 1919
Woosley, S. E., & MacFadyen, A. I. 1999, A&AS, 138, 499
Xu, D., Starling, R., Fynbo, J., et al. 2009, ApJ, 696, 971
Zenati, Y., Siegel, D. M., Metzger, B. D., & Perets, H. B. 2020, MNRAS, 499, 4097